Low voltage EPMA: experiments on a new frontier in microanalysis - analytical lateral resolution

2016 IOP Conf. Ser.: Mater. Sci. Eng. 109 012003

(http://iopscience.iop.org/1757-899X/109/1/012003)

IOP Conf. Series: Materials Science and Engineering **109** (2016) 012003 doi:10.1088/1757-899X/109/1/012003

Low voltage EPMA: experiments on a new frontier in microanalysis – analytical lateral resolution

J Fournelle[1], H Cathey[2,4], P T Pinard[3] and S Richter[3]

[1] University of Wisconsin-Madison, Department of Geosciences, 1215 W. Dayton Street, Madison, WI 53706, USA
[2] Arizona State University, LeRoy Eyring Center for Solid State Science, 901 S. Palm Walk, Tempe, AZ 85287-1704, USA
[3] RWTH Aachen University, Central Facility for Electron Microscopy (GFE), Ahornstrasse 55, 52074 Aachen, Germany

E-mail: johnf@geology.wisc.edu

Abstract. Field emission (FE) electron gun sources provide new capabilities for high lateral resolution EPMA. The determination of analytical lateral resolution is not as straightforward as that for electron microscopy imaging. Results from two sets of experiments to determine the actual lateral resolution for accurate EPMA are presented for Kα X-ray lines of Si and Al and La of Fe at 5 and 7 keV in a silicate glass. These results are compared to theoretical predictions and Monte Carlo simulations of analytical lateral resolution. The experiments suggest little is gained in lateral resolution by dropping from 7 to 5 keV in EPMA of this silicate glass.

1. Introduction

Recent papers [1-5] provide good summaries on field emission electron probe microanalysis (FE-EPMA). The most obvious advantage of the FE electron probe, relative to the more conventional W- and LaB_6-probes, is that the FE source produces a higher electron flux from a smaller source point and thus a smaller *initial* probe size, which itself is a function of both accelerating voltage on the gun as well as beam current. There is a 'sweet spot' for minimal spot size in terms of operating conditions (current work and informal discussion suggests 6 - 8 keV and ~ 10 nA). Nothing is gained by going to lower keV, as electrons with lower kinetic energy cannot be as tightly focussed, resulting in a wider beam. As beam current decreases, so does beam diameter but quantitative analysis requires abundant counts for good statistics, so generally one does not go below 10 nA unless it is feasible to count longer at lower beam current.

Operating at low keV introduces a plethora of issues which must be addressed, particularly carbon contamination [6] and complications of using non-traditional X-ray lines [7]. The issue of sample damage resulting from the intense FE beam impact has received slight attention, and will be addressed in a later document.

[4] Now at Central Analytical Research Facility, Institute for Future Environments, Queensland University of Technology, 2 George St., Brisbane, QLD 4000, Australia

The ability to acquire sharper images of nm-scale features does not equate to the ability to determine an accurate chemical composition of the same nm-scale feature. When considering X-rays generated by the electron beam, it is essential to appreciate the fact that virtually all of the X-rays collected by the detectors are generated at some depth within the sample (figure 1). The incident high energy electrons scatter and produce an interaction volume which has less to do with beam 'spot' size and much more to do with both the gun high voltage (keV) and the material composition (atomic number and density) and secondarily with beam current (nA).

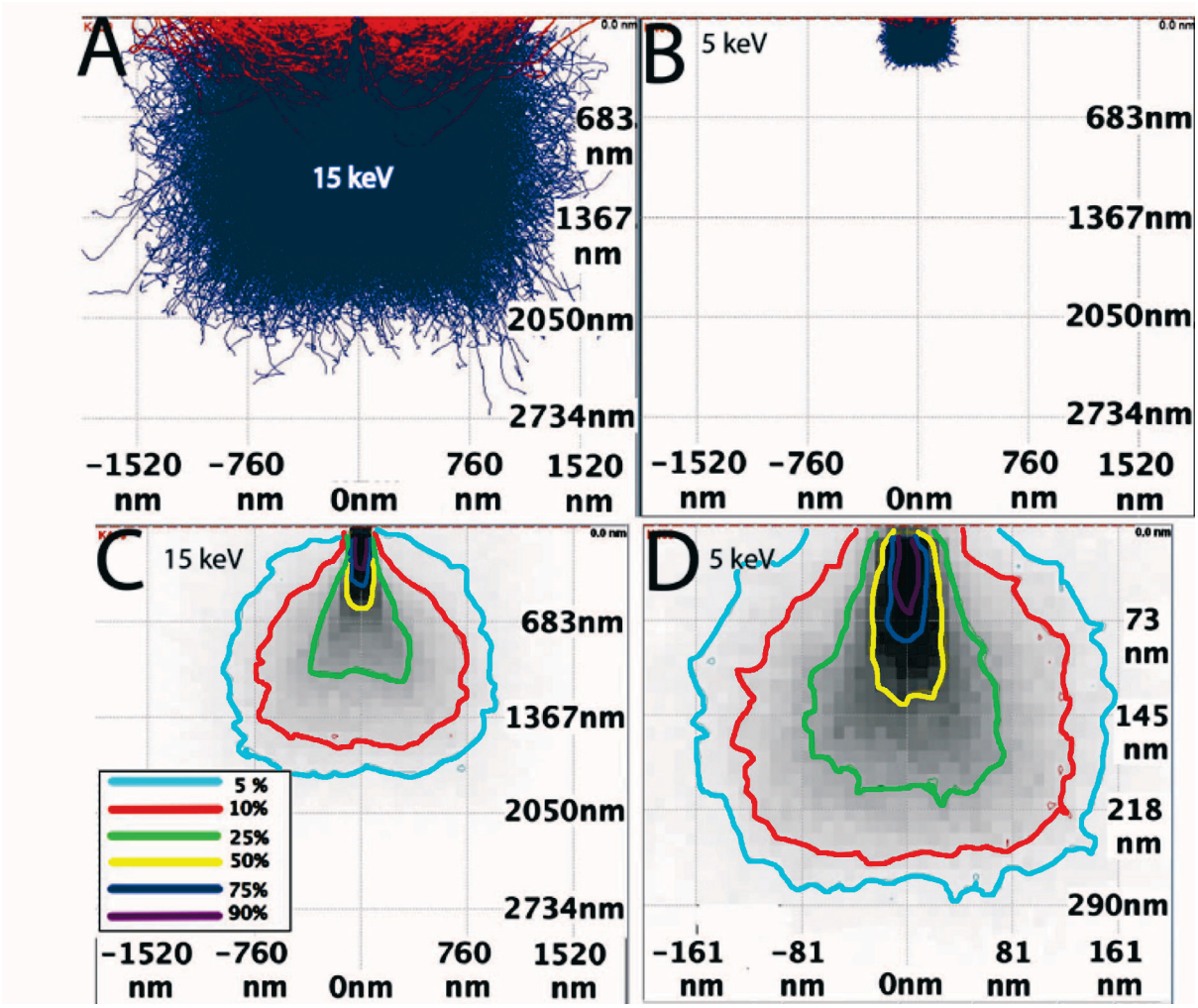

Figure 1. CASINO simulations of interaction volume in silicate glass K409, at 15 and 5 keV, with 10,000 trajectories, and 100 nm incident beam diameter. A-B-C at same scale, D magnified by a factor of 940 %. A, B indicate maximum extent of electron scattering. C, D show remaining energy of E_0 beam electrons in the glass. CASINO simulations indicate that higher energy electrons are concentrated in a more constrained cylindrical region (basis for the "low overvoltage approach" [1]), whereas lower energy electrons show more lateral scatter; for 15 keV beam electrons, this is for 4 keV and lower, whereas for 5 keV, this is for 1.2 keV and lower.

2. Background: X-ray analytical lateral resolution in low keV EPMA

The promise of low voltage FE EPMA is enhanced lateral resolution for quantitative analysis. With a field emission source, clearly electron (SE and BSE) image resolution is greatly improved. However, the problem of quantifying the lateral resolution of lower energy X-ray lines – including ones both traditionally and non-traditional used – assumes new and particular relevance.

2.1. Definitions of resolution

There is a potential for confusion regarding the word "resolution" in electron microanalysis, mainly because of the intimate association between electron microanalysis and electron microscopy imaging with secondary and backscattered electrons. The ability to "resolve" or distinguish two objects in an electron image is based on contrast measurements techniques.

Barkshire *et al.* [8] provided a good summary of the terminology of image resolution: (a) *point-to-point resolution* (an example being gold spheres on a graphite substrate) is defined as the minimum distance between two points over which the signal intensity drops by at least 75 % of the maximum intensity, and (b) *edge resolution* refers to the distance over which some percentage change in signal intensity occurs (e.g., 16 - 84%) in a scan over a sharp edge between two features.

Barkshire *et al.* [8] also give a definition of lateral resolution for EPMA, which is worth repeating:

> *... instead of simply being able to resolve the feature in an image, the entire X-ray information volume must be contained within the feature. Thus, for this purpose a more reasonable definition of lateral resolution is the diameter of a feature such that it will include some fraction of the total X-ray intensity, e.g., 99 %.*

2.2. X-ray range

Additionally, definition of X-ray range is important, as two concepts – X-ray range and X-ray lateral resolution – are sometimes used interchangeably, when they are not the same. X-ray range refers to an "average path length that electrons travel before slowing down to an energy equal to the excitation energy of the considered electron shell" [9]. As it encompasses all directions of electron travel within the sample, this solitary definition assumes that the average path length applies equally to vertical as well as lateral distances travelled. As Monte Carlo electron beam simulations show, this is true only for certain materials and clearly not all (e.g., in silicate minerals the beam penetrates relatively more deeply than wide, unlike in high Z metals). Moreover, as figure 1 shows, for a constant keV and material, the electron energy distribution is rather tightly constrained for higher energy X-ray lines, whereas for lower energy lines, the remnant electron energy is spread much wider, albeit deeper. Thus it is incumbent to appreciate that X-ray range values are involved with X-ray lateral resolution, but are not generally equivalent.

In his 1952 thesis, Castaing [10] proposed that X-ray range is determined by five factors according to the following equation:

$$R_x(nm) = \frac{33*A}{\rho*Z}(E_0^{1.7} - E_{Cr}^{1.7}) \quad (1)$$

where three of which are material dependent (atomic number, atomic weight, and density) the beam energy E_0; and the critical excitation energy E_{Cr} for a particular X-ray line of interest.

Since then, several other researchers have modified the equation: Anderson and Hasler [11], Reed [12], and Hovington *et al.* [13], but it retains the same overall formulation. In these formulations, the beam diameter is not a necessary factor for consideration.

2.3. X-ray lateral resolution

In the early 1960s when the newly invented electron probe microanalyser was being used to quantify elemental compositions of small objects, the question of exactly how small was the analytical volume came to the fore. Duncumb [14] proposed that to determine the analytical lateral resolution, the

calculated X-ray range value needed to be multiplied by a factor of 1.6. A decade and half later Reed [15] proposed that the X-ray range actually needed to be multiplied "by a factor of about 3".

Recently, Merlet and Llovet [9] re-addressed this question in two important ways. They included a term for the beam (spot) diameter, and they accounted for materials where electron penetration and scattering differ in the lateral and depth dimensions. This formulation of minimum analytical diameter includes an X-ray range value that is modified first by the depth of maximum X-ray generation (the deeper the maximum, the narrower the resolution, as seen in figure 1) and then includes the beam diameter. Their formulation for lateral resolution (R_s = diameter) uses Castaing's X-ray range (2) where R_x is that X-ray range, Z_m is the depth where the maximum distribution (i.e., phi-rho-Z) occurs, and d_0 is the beam diameter:

$$R_S = \sqrt{4(R_x - Z_m)^2 + d_0^2} \quad (2)$$

Another approach to estimating X-ray lateral resolution is Monte Carlo simulation, i.e., CASINO [16] and PENEPMA [17]. These simulations utilize a variety of approximations of the physics involved in the electron scattering and X-ray generation and absorption with the sample. Microanalysts commonly utilize these simulations to estimate the interaction volume prior to actually EPMA operation, to set the beam energy for a particular small size feature of interest.

The goal of this study is to utilize a well suited experimental material to generate data sets to evaluate predicted X-ray lateral resolution, fore quantitative resolution for accurate EPMA analysis, and compare estimates from both X-ray range and Monte Carlo estimates, with actual experimental data.

3. Experimental evaluation of X-ray lateral resolution

3.1. NIST K409, a useful material for FE EPMA

Several decades ago, the U.S. National Bureau of Standards (today NIST) developed several different reference materials as EPMA standards, and two glasses were publicized and distributed: K411 and K412 [18].

The K409 material was "re-discovered" at UW-Madison by John Fournelle when he took charge of the EPMA laboratory at the time Everett Glover retired from the position in 1992. A material labelled "NBS K409" with a nominal composition containing Na-Fe-Si-Al-O (table 1) was among the multitude of reference materials in the UW-Madison EPMA lab collection. After noting the ubiquity of micrometre-sized "fuzzy balls" in the material once it was mounted and polished for EPMA, Fournelle consulted Dale Newbury at NIST about the material, who explained that it was a "failed experiment." Apparently the oxygen partial pressure was too high and an iron-rich phase separated out. The glass was measured by EPMA using PROBE FOR EPMA's time-dependent-intensity correction (extrapolating to time = 0 to correct for elemental migration under the beam).

NIST K409 is a very useful material for assessing lateral resolution using low voltage EPMA by virtue of its unusual texture and composition [19]. It consists of iron oxide crystals that are rather uniform in size and shape (~ 800 nm maximum diameter quasi-octagons) that are densely distributed in a glass matrix (figure 2). Multiple measurements (table 2) suggest that dispersed within the iron-oxide crystals there is ~ 10 - 15 wt% of glass nano-inclusions. PEMEPMA calculations suggest that secondary fluorescence cannot account for this level of glass component measured in the crystals. Figure 2b shows tiny sub-100 nm-size regions of different intensity which would be consistent with trapped silicate liquid during rapid crystallisation (image is collected with SE detector, but backscattered electrons are also incident upon the detector, as evident in the contrast difference between the interstitial glass (dark grey) and the lighter grey Fe-oxide crystals

EBSD measurements were performed on the iron oxide crystals and the best fit (with low mean angular deviation, MAD) is consistent with the crystals being magnetite (figure 3).

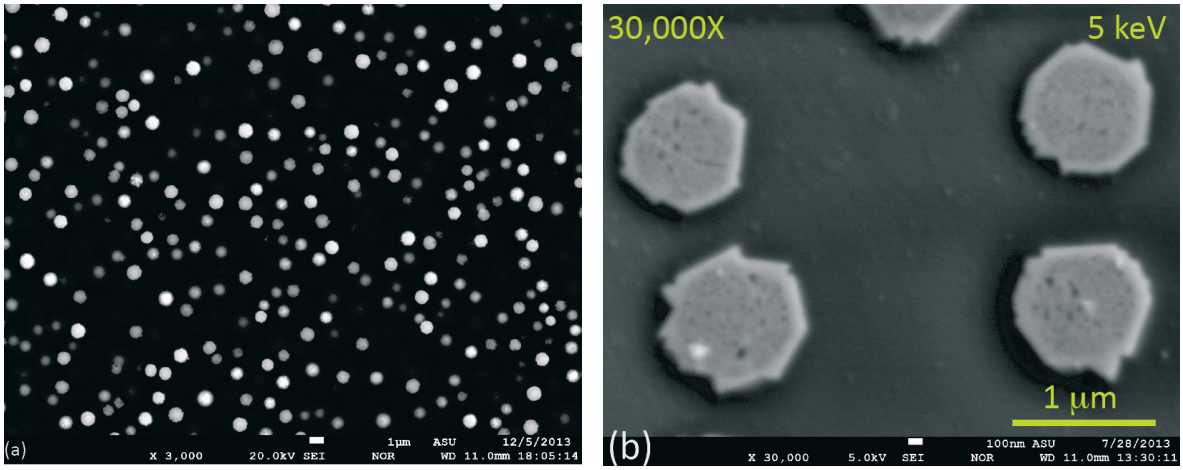

Figure 2. Two SEM images of NIST K409 glass. (a) At low magnification, the Fe-oxides appear circular, but at high magnification (b), they appear as equant crystals.

Table 1. Oxide weight% compositions for (1) original bulk material estimated by NBS (now NIST) for the glass synthesis, (2) EPMA defocussed beam (20 µm) analysis of the bulk material, and (3) EPMA measurement of the interstitial glass using a focussed beam and time dependent intensity (TDI) correction (PROBE FOR EPMA). (2) and (3) EPMA with the UW SX51, 15 keV, 10 nA.

	(1) Bulk - NBS/NIST nominal	(2) Bulk - EPMA defocussed	(3) Glass - EPMA TDI
SiO_2	55	56.6	59.9
Al_2O_3	15	15.1	17.0
FeO	20	15.7	6.4
Na_2O	10	9.8	10.8
MnO		0.2	
CaO		0.1	
Excess O		1.8	5.9
Total	100	99.3	100
(from)	on vial	SX51 2007	SX51 2012

3.2. Experiments with NIST K409: looking in the gaps

The Fe_3O_4 crystals are scattered throughout the NIST K409 glass with variable gaps separating them (figure 4). This experiment hypothesizes that at in regions furthest from any Fe-oxide crystals, the measured glass composition reflects the 'true' composition of the glass. Then at a series of smaller inter-crystal spacing, one would measure glass compositions that would show "contamination" by the adjacent Fe-oxide crystals. And at the point where the effect of the adjacent Fe-oxides were not observed, would then be an experimental determination of the analytical lateral resolution of the X-ray lines being evaluated: Si-Kα, Al-Kα and Fe-Lα. Na-Kα was attempted but unsuccessful (see below).

Table 2. Quantitative FE-EPMA of magnetite in NIST K409 using the Fe-Lα X-ray line. Results in (a) and (b) include direct measurement of oxygen on the RWTH-Aachen JEOL 8530F (O = excess measured oxygen). (c) EPMA using Arizona State University (ASU) JEOL 8530F with oxygen calculated by stoichiometry. Fe recast as Fe_3O_4. Although there are some discrepancies in Si and Al between the two datasets at 5 keV, each is internally consistent and shows significant measurement of Si and Al. Monte Carlo simulations by PENEPMA do not predict this amount of Si and Al by either primary or secondary fluorescence. A possible explanation for Si and Al differences would be variable amounts of nanoscale glass trapped within the Fe_3O_4 crystals.

(a) 4 keV 10 nA (RWTH Aachen JEOL 8530F)

Analysis#	SiO2	Al2O3	Fe3O4	MgO	CaO	Na2O	K20	excess O	Total
1	10.50	4.23	87.9	0.08		1.02		-1.67	102.1
2	11.07	3.60	87.2	0.08		1.06		2.12	100.9
3	9.86	3.88	85.4	0.12		0.93		0.00	100.2
4	11.14	4.29	85.3	0.17		1.06		-1.32	100.6
5	11.32	4.03	85.6	0.06		0.59		-1.64	99.9
Average	10.78	4.01	86.3	0.10		0.93		-1.35	100.7
Std Dev	0.60	0.28	1.2	0.04		0.20		0.81	0.8

(b) 5 keV 10 nA (RWTH Aachen JEOL 8530F)

Analysis#	SiO2	Al2O3	Fe3O4	MgO	CaO	Na2O	K20	excess O	Total
1	10.40	4.08	83.4	0.16	0.52	0.77	0.00	-0.06	99.2
2	9.23	2.16	88.8	0.12	0.08	0.64	-0.06	-0.93	100.0
3	9.58	2.71	87.4	0.09	-0.14	0.87	0.01	-0.70	99.8
4	10.17	3.01	86.9	0.18	-0.04	0.92	-0.05	-0.52	100.6
5	10.40	2.65	88.2	0.19	0.16	0.83	0.28	0.09	102.7
6	10.41	3.25	84.7	0.11	0.01	1.01	-0.07	-0.17	99.2
7	9.82	3.29	86.7	0.16	0.34	0.95	-0.02	-0.99	100.2
8	10.70	2.79	86.0	0.13	0.30	0.75	0.06	-0.29	100.4
9	9.22	2.80	88.7	0.07	0.30	0.86	-0.15	-0.94	100.9
Average	9.99	2.97	86.7	0.13	0.17	0.84	0.00	-0.50	100.3
Std Dev	0.55	0.54	1.8	0.04	0.21	0.11	0.12	0.41	1.1

(c) 5 keV 10nA (ASU JEOL 8530F)

Analysis#	SiO2	Al2O3	Fe3O4	MgO	CaO	Na2O	K20	excess O	Total
1	7.36	2.11	89.3	0.02		0.72			99.5
2	7.86	2.19	86.1	0.19		0.36			96.7
3	7.20	2.27	85.6	0.20		0.65			95.9
4	6.48	2.00	83.5	0.21		0.70			92.9
5	7.06	2.22	89.5	0.31		0.61			99.7
6	7.32	2.35	89.1	-0.10		0.69			99.3
7	6.73	2.07	90.6	0.16		0.52			100.0
8	7.52	2.25	85.5	-0.20		0.63			95.7
9	6.99	1.74	91.5	0.02		0.65			100.9
10	6.86	1.94	88.9	-0.04		0.59			98.2
11	7.16	2.15	89.0	-0.02		0.66			98.9
Average	7.14	2.12	88.0	0.07		0.62			98.0
Std Dev	0.38	0.18	2.5	0.16		0.10			2.4

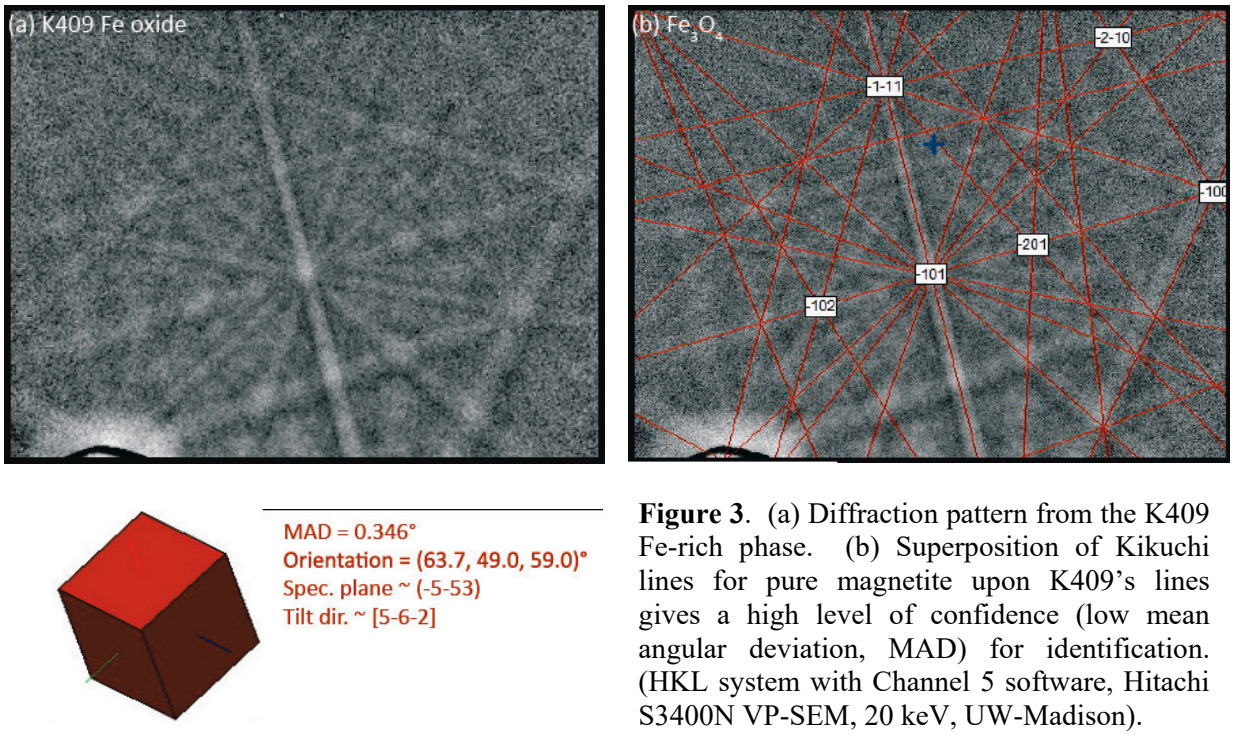

Figure 3. (a) Diffraction pattern from the K409 Fe-rich phase. (b) Superposition of Kikuchi lines for pure magnetite upon K409's lines gives a high level of confidence (low mean angular deviation, MAD) for identification. (HKL system with Channel 5 software, Hitachi S3400N VP-SEM, 20 keV, UW-Madison).

An additional test would be whether a given X-ray line intensity reached a plateau in the gap between two Fe-oxides, suggesting little contribution from the adjacent phases.

A key part of this project is to evaluate the various theoretical predictions for X-ray analytical resolution with the experimental results. In addition to the X-ray range calculation and predictions using the multiplicative factors for X-ray ranges of Duncumb and of Reed, CASINO and PENEPMA models were performed, all using the glass composition in table 1 and a density of 2.6 g/cm^3.

The experiments were performed at 5 and 7 keV with the UW-Madison SXFive FE probe (#944) with faraday cup current of 10nA. A focussed beam was used with a measured 80 - 100 nm diameter. Beam deflection was used with ~ 100 nm steps. The liquid nitrogen (LN)-anti-contamination plate was in operation, and generated some small vibrations (not believed to be of major significance here). The NIST K409 glass was mounted in epoxy, polished down to 0.3 µm diamond, and coated with 4 nm of Ir.

Two series of experiments were performed. The initial ones were a series of EPMA line profiles through the centres of the largest of these crystals – looking for the smallest gap that gives the same X-ray intensity as seen far from the crystals. This is an indication of the ability to resolve the intervening glass composition without direct contribution from the iron oxide crystals.

Upon further evaluation of the counting statistics of the first set of experiments, a second series were run, for long count times as well as duplicate spectrometers for Si, with a stationary beam at the midpoint between series of pairs of the crystals.

3.2.1. Line scans. Figure 4 shows line scans along pairs of magnetite crystals with different spacings. Counts were collected for 5 seconds per spot, at ~ 100 nm distance between analyses. Background counts were not subtracted; gross counts were plotted. Na loss was rapid and no evaluation of Na-Kα resolution was attempted. Any Si and Al 'grow in' (increase in counts) did not appear to affect the results as the Si, Al and Fe counts between sufficiently widely spaced crystals were similar in magnitude to the distant glass count levels for these elements.

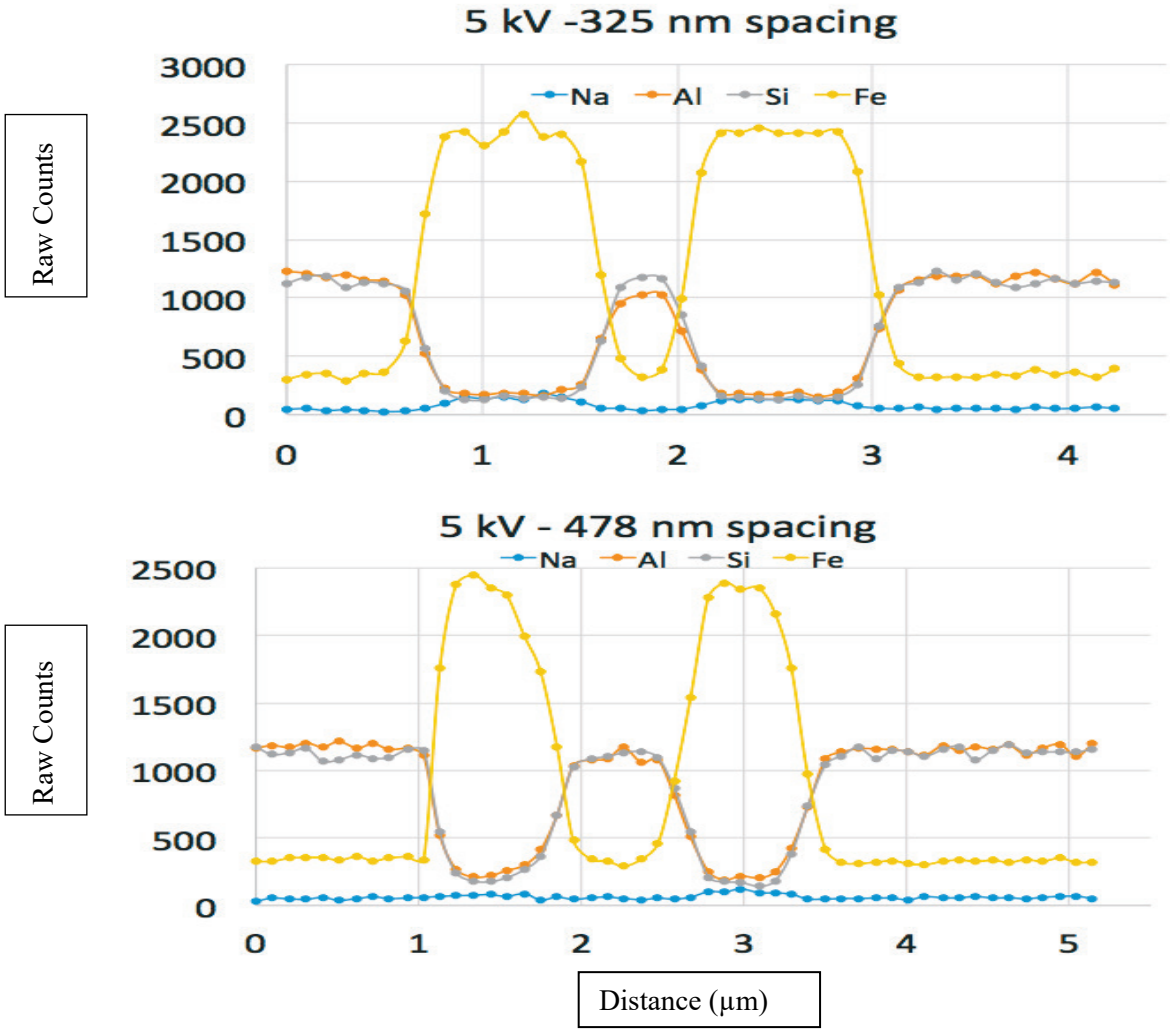

Figure 4. Examples of two of the traverses at 5 keV, through the centres of Fe_3O_4 crystals. Measurements with CAMECA SXFive FE at University of Wisconsin-Madison.

In the Figure 4 line scans, "spacing" refers to the measured distance between Fe-oxide crystals, measured from the closest edges using secondary electron images, and using the largest and equal sized crystals.

In the initial experiments, the numbers of traverses being evaluated were: 7 at 5 keV, and 10 at 7 keV. Shown below in figure 4 are two traverses at 5 keV, where one spacing shows some clear interaction with the adjacent Fe_3O_4 crystals as indicated by the reduced intensity of Al-Kα (orange dots) relative to that at distance. For the wider spacing, the Al-Kα matches that at distance.

The ratios in table 3 were determined by taking the maximum X-ray intensity for Al-Kα, Si-Kα and Fe-Lα on the glass in the gap between two Fe_3O_4 crystals, and dividing by the glass X-ray intensity 1 - 1.5 µm "far away" from the crystals.

An evaluation of the precision of the measurements based upon counting statistics shows that while a qualitative estimate can be made of analytical resolution based on these results, the error bars are large: taking the traverses at 7 keV as an example, for a 2 sigma error there is variability in the Al and Si-Kα measurements of ~7% (thus values from 0.93 - 1.08 are indistinguishable from 1.00); variability

Table 3. Results from 5 and 7 keV experiments, with ratios relative to glass composition in regions far from the Fe_3O_4 crystals.

5 keV	X-ray intensity relative to far away		
spacing nm	Al Kα	Si-Kα	Fe Lα
300	0.81	0.91	1.20
325	0.87	1.03	0.95
360	0.97	0.97	1.03
416	0.81	0.87	0.91
478	0.94	0.99	0.98
490	1.01	0.96	0.99
528	0.95	1.00	1.00
7 keV	X-ray intensity relative to far away		
spacing nm	Al-Kα	Si-Kα	Fe Lα
454	0.92	0.96	1.19
485	0.88	0.94	1.18
571	0.95	0.95	1.05
586	0.93	0.97	1.18
670	0.85	0.99	0.87
675	0.93	0.97	0.87
686	1.01	0.99	0.96
749	0.98	1.01	0.93
776	0.98	1.01	0.89
882	1.01	0.99	0.96

in Fe-Lα is worse, with errors reaching 20 %. These errors were calculated by taking, for each measurement, the average value of the gap measurements (i.e., one 5 second count), and then determining the 2 sigma value.

3.2.2. Point measurements. In order to reduce the counting statistical error in the measurements, an additional experiment was designed. In order to determine whether a point midway between two Fe_3O_4 crystals encompassed only the excitation volume of the glass and not the Fe-oxides, spot analyses with an on-peak counting time of 50 seconds were performed at each of X midpoints between crystals (20 spots for the 5 keV and 30 for the 7 keV experiments), representing a range of midpoint distances between crystals of ~ 300 - 900 nm. Similarly, counts were collected for 50 seconds in at several spots in glass that were distant from obvious Fe-oxides. As before, a beam current of 10 nA was used, with spot size of ~ 100 nm. However, here 3 spectrometers (2 LPETs + 1 TAP) counted simultaneously on Si-Kα and their counts were summed, yielding a 1 sigma counting statistical error of 0.4 % / 0.3 % (5 keV / 7 keV values). Al-Kα (on a LTAP) yielded a counting statistics error of 0.5 % / 0.4% and Fe-Lα (on a PC1 60 Å W/Si) had a 1 sigma statistical error of 1.3 % / 1.1%. Results are shown in figure 5.

These experiments provide additional data to consider the analytical lateral resolution in silicate glasses similar to the K409 composition. Clearly it lacks other cations commonly abundant in many natural glasses as well as in common silicate minerals (e.g., Mg, Ca); nevertheless these data can be used to evaluate the theoretical analytical lateral resolution for this composition.

With respect to the experiments at 7 keV at 800 nm and higher, the normalized value for Si-Kα counts is at or very close to 1.00, whereas from 600 - 800 nm values range from 0.95 to 1.00. The data for Al-Kα are roughly similar to those for Si-Kα, but with more scatter down to 0.90. Data for

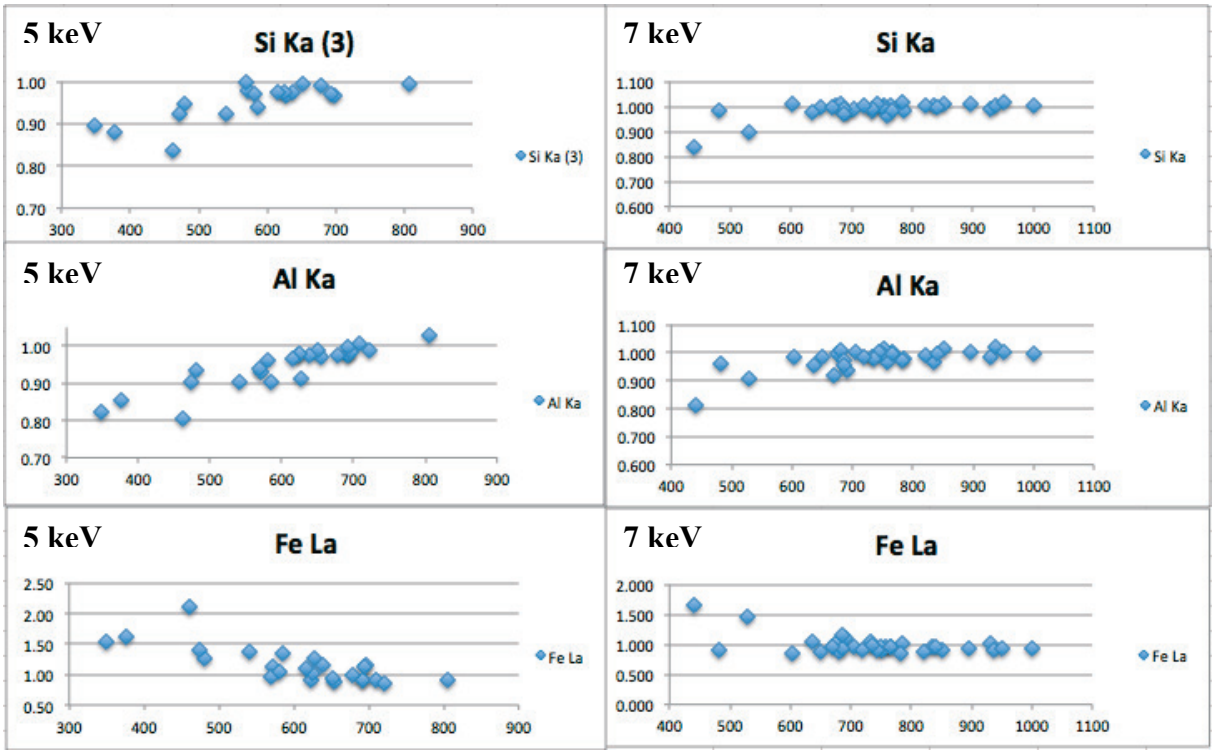

Figure 5. Plots of counts on NIST K409 glass normalized to glass composition far from Fe_3O_4 crystals. X-axis is nanometre spacing between Fe-oxide crystals.

Fe-Lα follow this general behaviour (glass regions representing shorter midpoint distances clearly contain Fe from the adjacent Fe-oxides). One would conclude from these data that the minimum analytical lateral resolution for these X-ray lines is somewhere between 600 - 700 nm. One would expect the lower energy Al-Kα and Fe-Lα lines (compared with Si-Kα) to have decreased (wider) lateral resolution, but the data do not permit such a refined determination (and the issue of statistics must play a role, particularly for the lower count rate Fe-Lα).

An obvious point of concern is whether Fe-oxides reside within the sample interaction volume just below the surface. Their presence was detected in some of the first experiments, by excursions of count intensities in some of the traverses. In the second series of experiments, the evidence would include elevated Fe compared with lowered Al and Si counts, and that is seen in some of the data around 700 nm.

At 5 keV (figure 5), the data for all of the X-ray lines – Si-Kα, Al-Kα and Fe-Lα – suggest a minimum lateral resolution of 575 - 650 nm.

4. Theoretical results using NIST K409

4.1. CASINO modelling

CASINO v2.42 [13] was run assuming a single phase (i.e., bulk K409 glass) at 5 and 7 keV, and the results for X-ray radial distribution were output and evaluated to determine the lateral distance (2 times the radial distance) at which 99.9 % of the X-ray intensity was contained. Figure 6a shows the result for Si-Kα at 5 keV from the CASINO simulation.

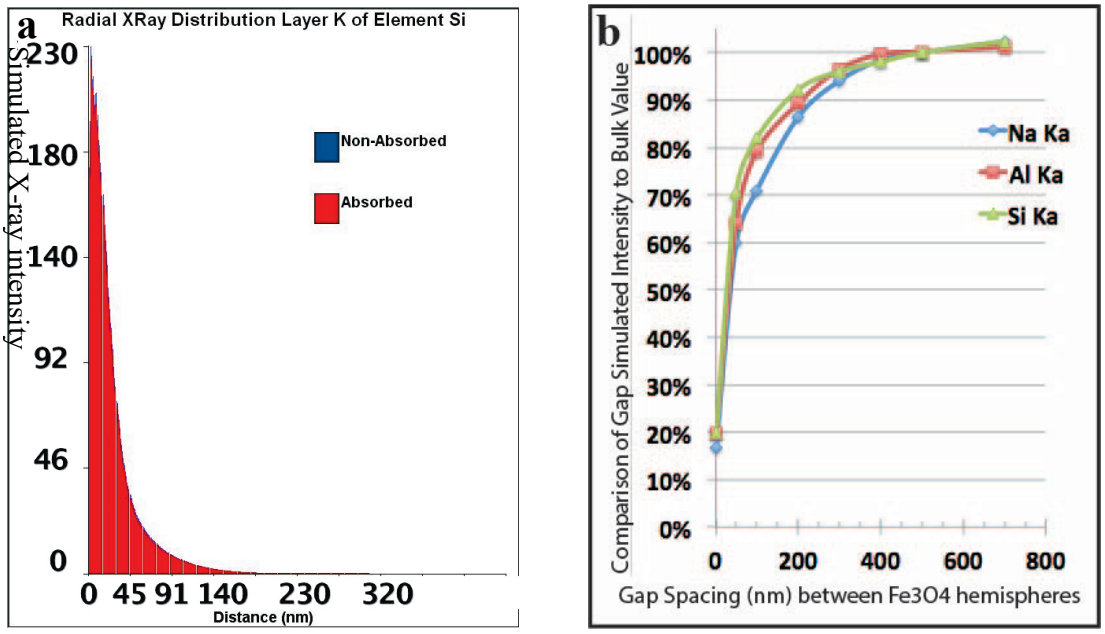

Figure 6. Monte Carlo simulations of low voltage EPMA of K409 glass. (a) Left, CASINO X-ray radial distribution for 5 keV simulation of Si-Kα in bulk glass K409 with beam diameter of 100 nm. The CASINO model shows negligible absorption of Si-Kα. (b) Right, PENEPMA 5 keV simulation of X-rays detected with beam halfway between two 800 nm Fe-oxide hemispheres, with the annular detector at a 40° take off angle.

4.2. PENEPMA modelling

PENEPMA Monte Carlo modelling allows a full simulation of a geometry of two 800 nm diameter Fe_3O_4 hemispheres at variable spacings in a matrix of K409 glass composition. Simulations were run for 18 - 24 hours. Figure 6b shows the results of the PENEPMA 5 keV set of simulations. The data are all from simulations using actual K409 glass composition (table 1, 3rd column). Nine simulations were done: 8 for spacings from 0 nm (touching) to 700 nm, and one for bulk material – which was the reference to which each of the various spacings was compared. Thus, at 200 nm spacings, the simulated X-ray intensities, relative to what they 'should' be, is around 87 % for Na, ~ 89 % for Al and ~ 91 % for Si. At 0 nm spacing, the spheres touch at a point and there is exposed glass, so the value is 15 – 20 %, not zero. (The 2014 version of PENEPMA provides a nice quick graphical representation of 3D X-ray generation within the target material, but is not shown here. The approach used here, while slower, includes the absorption at the given detector take-off angle, and is more directly comparable with the actual experimental data).

PENEPMA modelling here indicated that all 3 elements reach a value of 100 % of the bulk K409 composition only when the spacing is at 500 nm. Experiments were only done in no tighter than 100 nm increments, and optimally future work would include tighter spacing (e.g., 50 nm steps near the putative resolution point).

This PENEPMA modelling also indicates that there should be less than ~ 1 % secondary fluorescence (including continuum) involvement.

5. Experimental versus theoretical results using NIST K409

Table 4 compares the results of theoretical calculations with experimental results on analytical lateral resolution at 5 and 7 keV. Key observations include:

1. For silicate glass of K409 composition, all the calculated X-ray ranges using published formulations at 5 keV are smaller than the observed X-ray analytical lateral resolution, whereas for 7 keV, those of Castaing and Anderson-Hasler are close to the experimental values.
2. The formulations of Duncumb and of Reed do not match the experimentally observed lateral resolution (either over or underestimate).
3. Merlet and Llovet's [9] estimation is close for the 5 keV case (using the CASINO depth of maximum phi-rho-Z distribution) but overestimates lateral resolution in the 7 keV case.
4. PENEPMA calculations agree closely with experimental measurements 7 keV, but underestimate by ~ 20 % for 5 keV.
5. CASINO's "X-ray radial distribution" (multiplied by 2 to give an analytical resolution value) is actually close to the Castaing X-ray range value for both 5 and 7 keV, and is lower than the experimentally observed 5 keV lateral resolution, but matches that for 7 keV.

Table 4. Comparison of experiments at 5 and 7 keV with various estimations of analytical X-ray lateral resolution, for Si-Kα, Al-Kα and Fe-Lα in K409 glass, using various published formulations and results from Monte Carlo simulations. For Merlet-Llovet formula, (a) uses phi-rho-Z max from CASINO, (b) uses phi-rho-Z max from Merlet (pers. comm.). PENEPMA for Fe-Lα not included due to poor statistics.

X-ray ranges	5 keV Al-Kα	5 keV Si-Kα	5 keV Fe-Lα	7 keV Al-Kα	7 keV Si-Kα	7 keV Fe-Lα
Castaing 1952	351	321	405	664	625	730
Anderson-Hasler '66	322	311	352	602	590	632
Reed '66	273	257	314	491	475	531
Hovington et al '97	297	281	333	558	543	1065
Analytical resolution						
Duncumb (x1.6)	437	411	502	785	759	849
Reed (x3)	820	772	940	1472	1424	1593
Merlet-Llovet '12 (a)	578	512	619	989	909	1065
Merlet-Llovet '12 (b)	515	465	607	974	900	1091
PENEPMA (100 %)	500	500	*	700	700	*
CASINO (99.9 %)	360	360	436	674	674	755
K409 point experiments	575-650	575-650	575-650	600-700	600-700	600-700

6. Conclusions

The theoretical estimates of X-ray ranges indicate that there is a significant improvement in dropping from 7 to 5 keV. Similarly, the theoretical estimates for analytical resolution also indicate the same improvement in dropping from 7 to 5 keV. However, the K409 experiments show that there may be only a slight improvement to be gained by operating at 5 keV versus 7 keV. Any gain in a slightly smaller degree of electron scattering is offset by beam broadening (and perhaps issues of surface contamination).

With respect to Si-Kα and Al-Kα lines versus the lower energy Fe-Lα line, the theoretical analytical volume encompassing excitation of the Fe-Lα line would be larger than that for only the Si-Kα and Al-Kα lines, given that less energy is needed to generate the Fe-Lα line. All the Fe-Lα

X-ray lateral estimates in Table 4, based on theoretical calculations, show such a results. All these cited values (PENEPMA not included there), have one thing in common – they consider only one phase, the glass, and not the adjacent Fe-oxides.

This predicted wider Fe-Lα X-ray lateral resolution is not observed in the experiments. Absorption of the Fe-Lα X-ray energy may account for this observation, such that resolution of Fe-Lα ends up matching that of Si-Kα and Al-Kα. This behaviour is actually beneficial for silicate analysis where one would like the different elemental X-ray intensities contributing to the compositional analysis by EPMA to represent the same volume.

Further work needs to be done to better understand the behaviour of the low energy Fe-Lα X-ray line here. The SE image (figure 2) may indicate some polishing-induced relief between the glass and the Fe-oxides, and it would be helpful to check to verify this. If relief is present, then any impact on X-ray intensity could be modelled in a more complex Monte Carlo geometry. And longer PENEPMA models could be run to achieve the required statistical significance for modelling the Fe-Lα intensity therein, where the multi-phase (glass plus two Fe-oxides) assemblage could be simulated.

Acknowledgements
The following researchers have been generous with their comments and advice concerning low voltage EPMA over the past several years: Xavier Llovet, Phil Gopon, Michel Outrequin, Chrystel Hombourger, Dieter Rhede, John Armstrong, Peter McSwiggen, Stuart Kearns, and Chi Ma. Two anonymous reviewers are thanked for their comments. JF acknowledges NSF-MRI award EAR-1337156 to UW-Madison for the SXFive FE electron probe.

References
[1] McSwiggen P 2014 *IOP Conf. Ser.: Mater. Sci. Engng*. **55** 012009
[2] Hombourger C and Outrequin M 2013 *Microscopy Today* **21**(3) 10
[3] Pinard P T and Richter S 2014 *IOP Conf. Ser.: Mater. Sci. Engng*. **55** 012016
[4] Rinaldi R and Llovet X 2015 *Microsc. Microanal.* **21** 1053
[5] Berger D and Nissen J 2014 *IOP. Conf. Ser.:Mater. Sci. Engng*. **55** 012001
[6] Buse B and Kearns S 2015 *Microsc. Microanal*. **21** 594
[7] Gopon P, Fournelle J, Sobol P E and Llovet X 2013 *Microsc. Microanal.* **19** 1798
[8] Barkshire I, Karduck P, Rehbach W P and Richter S 2000 *Mikrochim. Acta* **132** 112
[9] Merlet C and Llovet X 2012 *IOP Conf. Ser.: Mater. Sci. Engng*. **32** 012016
[10] Castaing R 1952 PhD-thesis. *Publication ONERA* no. 55
[11] Anderson C A and Hasler M E 1966 *Proc. 4th IXCOM*. (Castaing R, Deschamps P and Philibert J; Eds.) (Paris: Hermann) p 310
[12] Reed S J B 1966 *Proc. 4th IXCOM*. (Castaing R, Deschamps P and Philibert J; Eds.) (Paris: Hermann) p 339
[13] Hovington P, Drouin D, Gauvin R and Joy D C 1997 *Microsc. Microanal. **3** suppl* 2 885
[14] Duncumb P 1960 in: *X-ray Microscopy and X-ray Microanalysis. Proc. 2nd Intl Symposium*. (Engstrom A, Cosslett V and Pattee H; Eds.) (Amsterdam: Elsevier) 364
[15] Reed S J B 1975 *Electron Microprobe Analysis* (Cambridge: Cambridge University Press)
[16] Hovington P, Drouin D and Gauvin R 1997 *Scanning* **19** 1-14
[17] Salvat F, Fernandez Varea J M and Sempau J 2013 *PENELOPE - A code system for Monte Carlo Simulation of Electron and Photon Transport.* (Issy-les-Moulineaux, France: OECD/Nuclear Energy Agency)
[18] Marinenko R B 1982 Standard Reference Materials: Preparation and Characterization of K-411 and K-412 Mineral Glasses for Microanalysis SRM 470. *NBS Special Publication* 260-274.
[19] Cathey H, Gopon P and Fournelle J 2013 *AGU Fall Meeting Abstracts* 2793